Title

Pseudo-Three-Dimensional Back-Analysis of Rainfall-Induced Landslides in Utuado, Puerto Rico

Journal

GEO-CONGRESS 2024: GEOTECHNICS OF NATURAL HAZARDS, 349(GSP 349)

ISSN

0895-0563

Authors

Kassem, Mirna
Gong, Weibing
Zekkos, Dimitrios
et al.

Publication Date

2024-02-22

DOI

10.1061/9780784485316.060

Pseudo-Three-Dimensional Back-Analysis of Rainfall-Induced Landslides in Utuado, Puerto Rico

Mirna Kassem, S.M.ASCE[1]; Weibing Gong, Ph.D., A.M.ASCE[2];
Dimitrios Zekkos, Ph.D., P.E., M.ASCE[3]; Marin Clark, Ph.D.[4]; and Stephen Hughes, Ph.D.[5]

[1]Dept. of Civil and Environmental Engineering, Univ. of California, Berkeley, CA.
Email: kassem_mirna@berkeley.edu
[2]Dept. of Geosciences and Geological and Petroleum Engineering, Missouri Univ. of Science and Technology, MO. Email: weibing.gong@mst.edu
[3]Dept. of Civil and Environmental Engineering, Univ. of California, Berkeley, CA.
Email: zekkos@berkeley.edu
[4]Dept. of Earth and Environmental Sciences, Univ. of Michigan, Ann Arbor, MI.
Email: marinkc@umich.edu
[5]Dept. of Geology, Univ. of Puerto Rico, Mayaguez, PR. Email: kenneth.hughes@upr.edu

ABSTRACT

Regional slope stability analyses can provide a system-level assessment of landslide susceptibility. This study aims to develop a regional back-analysis model for rainfall-induced landslides to compute ground shear strength that can be used for landslide prediction. Most commonly, mechanistic-based models for regional slope stability consist of simplified one-dimensional (1D) analyses compared to more realistic three-dimensional (3D) procedures. A pseudo-3D methodology is applied on 788 landslides over two 2.5 km^2 areas in the plutonic rocks of the Utuado Batholith. First, an infinite slope stability triggering model is applied on a 1 m-resolution digital elevation model (DEM) to identify the triggering grid cells. A spatial 3D projection procedure is then implemented to generate 3D landslides with defined location, area, and volume. Two inversion procedures are considered herein: inversion against landslide area density and inversion against individual landslides. Unlike inversion against landslide area density, inversion against individual landslides generated good match in landslides' locations and sizes and resulted in lower scatter in regional strength estimates. The average back-calculated cohesion and friction angle were c' = 1 kPa, ϕ' = 57° and c' = 2 kPa, ϕ' = 56° for the first and second study areas, respectively. Inversion against landslides' volumes in addition to their areas and centroid locations reduced the uncertainty in the triggering depth and modeled shallower landslides, which better matched the mapped landslides.

INTRODUCTION

Several empirical models that incorporate threshold rainfall intensities and durations to trigger landslides have been developed (Segoni et al., 2018). However, these empirical models, unlike mechanistic models, provide little theoretical basis for understanding the physical mechanisms of rainfall-induced landslides and the interaction between the different hydrological, geologic, and topographic parameters (Schilirò et al., 2015). Back-analysis of mapped landslide inventories from natural disasters can be used to calculate the shear strength parameters using methods that can vary from simple one-dimensional (1D) to more complex three-dimensional (3D). Back-analyses approaches are particularly useful for large areas where extensive field and laboratory tests are difficult to conduct (Gong et al., 2023).

In this study, we present a mechanistic pseudo-3D regional back-analysis method for rainfall-induced landslides developed based on hydrological and topographic parameters. These parameters are used as input into a 1D slope stability analysis accompanied with a spatial projection of the landslide geometry to form a 3D landslide with a well-defined location and size. Two inversion procedures are presented and compared herein: inversion of landslides to match the average landslide area density and inversion with the goal to match individual landslides. A total of 788 mapped landslides induced by Hurricane Maria in Utuado in Puerto Rico were used to back-calculate the shear strength parameters (U.S. Geological Survey, 2020). The inversion against individual landslides method was implemented twice: In one case the mapped volumes of landslides were used in the inversion, while in the second case, the volumes of the landslides were not included in the inversion analyses, with the goal to assess the importance of incorporating volumes of mapped landslides in the back-calculation of strength parameters.

STUDY AREA

More than 70,000 landslides occurred in Puerto Rico during Hurricane Maria (Hughes et al., 2019). The focus of this study is the Utuado area in central Puerto Rico where the landslide area density was found to be highest and exceed 100 landslides/km^2 (Hughes and Schulz, 2020). Two 2.5-km^2 study areas (Figure 1) were selected for inversion. In this study, we use a high-quality mapped landslide inventory that includes landslide polygon location and source area (U.S. Geological Survey, 2020). In addition, we use a 1m-resolution pre-Hurricane DEM generated based on a LiDAR survey (U.S. Geological Survey, 2017). The geology of the study area consists of plutonic rocks of the Utuado Batholith dating back to the Cretaceous era. The unit consists mostly of massive granodiorite with some quartz diorite, quartz monzonite, diorite, and gabbro.

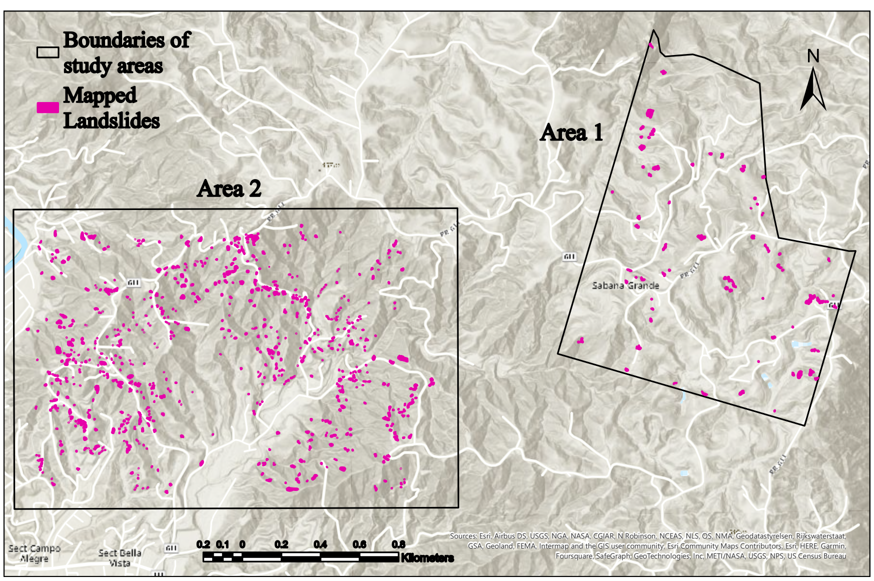

Figure 1. Mapped landslides in Utuado region

Volumes have been measured for 8,433 individual landslides in the broader area using LiDAR differencing in the same geologic unit (Bayouth-Garcia, pers. comm, 2023). A powerlaw volume-area relationship based on those landslides is used to describe the volume-area relationship for the mapped landslides. Hence, volumes of the mapped landslides were calculated as:

$$V = 0.53 * A^{1.16} \tag{1}$$

where V is the mapped volume and A is the source area of the mapped landslide.

MODEL FORMULATION

The two inversion procedures generate landslides in a similar manner but differ in the matching criteria used for identifying combinations of effective cohesion (c'), effective friction angle (ϕ'), pore water pressure (R_u), and triggering depth (z) that match the field observations. Landslides are generated based on two steps: (1) identification of triggering points of landslides based on a 1D slope stability analysis and (2) generation of 3D landslide failure surfaces through a spatial projection of the landslide geometry using geomorphic characteristics and a geometric rule (Gallen et al., 2015; Gong et al., 2023).

1D Slope Stability Analysis

A 1D analysis method is first applied to identify the triggering grid cells based on the infinite slope stability limit equilibrium. The infinite slope assumption is reasonable for simulating shallow and translational soil slips with a maximum depth of approximately 1.5–2m (Godt et al., 2008) which was mostly the case for the landslide inventory used in this study. Potential triggering grid cells are defined as cells with a factor of safety (F_s)<1. A F_s is defined as the ratio of the effective shear strength to the driving shear stress. The F_s of each grid cell is calculated using Eq. (2), which is derived based on the 1D slope model shown in Figure 2 (Duncan et al., 2014):

$$F_s = \frac{c'}{\gamma z}\frac{2}{\sin(2\beta)} + \left[\cot(\beta) - R_u\big(\cot(\beta) + \tan(\beta)\big)\right]\tan(\phi') \tag{2}$$

where c' and ϕ' are the effective cohesion and friction angle respectively, β is the slope angle, γ is the material unit weight, z is the vertical depth of the failure plane, and R_u is the pore water pressure coefficient defined as (Bishop and Morgenstern, 1960):

$$R_u = \frac{u}{\gamma z} \tag{3}$$

where u is the pore water pressure, U is the pore water force, W is the weight of the material, N is the normal force, and T is the shear resistive force.

A total material unit weight of 22 kN/m^3 is assumed. The initial conditions prior to the precipitation event are represented by an R_u value of zero. For these conditions, the model ensures that at least 95% of the grid cells are stable. Only mapped landslides with areas greater than 3 m^2 (i.e., size of 3 grid cells in a 1m-resolution DEM) were considered in the analysis. Hence, out of the 827 landslides, 788 landslides were used in the inversion analysis.

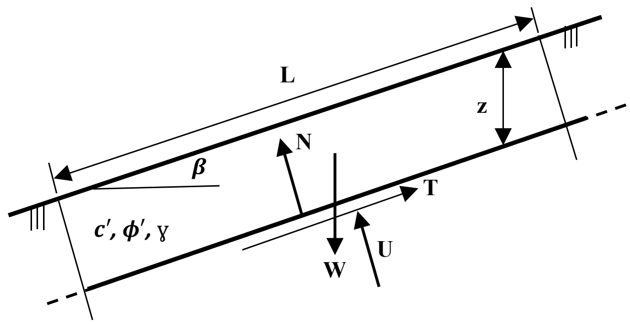

Figure 2. Infinite 1D slope stability model

3D Landslide Generation

Given all the potential triggering cells for one combination of c', ϕ', R_u, and z, landslides are generated from the cell with the highest accumulation area first. The 1D slope stability analysis is expanded into a 3D landslide geometric approximation based on an approach suggested by Gallen et al. (2015) and implemented by Gong et al. (2023) for earthquake-induced landslides. This approach uses triggering grid cells as the initiation points to populate the topography with landslides with well-defined areas and volumes. Given a 1m-resolution DEM, a modeled landslide should consist of more than 3 grid cells to be acceptable in this model. Of the generated landslides, the landslide with minimum total error is accepted per each combination.

INVERSION PROCEDURE

For both inversion procedures, c' is varied from 0 to 100 kPa with increments of 3 kPa, ϕ' is varied from 5° to 70° with increments of 3°, and z is varied from 0.5m to 10 m with increments of 0.5 m. R_u is varied from 0.05 with increments of 0.05 to a maximum R_u value of 0.45, which corresponds to the saturation of the slope up to the ground surface per Eq. (3). Acceptable combinations of c', ϕ', R_u, and z are those that give a minimum total error. For each acceptable combination, the effective normal stress (σ') and shear strength (τ) are calculated following the Mohr Coulomb failure criterion as:

$$\sigma' = (1 - R_u) * \gamma * z * \cos^2(\beta) \quad (4)$$

$$\tau = c' + \sigma' \tan(\phi') \quad (5)$$

Inversion against Landslide Area Density

The matching criterion followed in this inversion procedure is based on the landslide area density calculated as the ratio of the total area of the landslides to the total area of the studied region. The relative error between the mapped and modeled landslide area densities (LAD_{mapped} and $LAD_{modelled}$ respectively) is calculated as:

$$\varepsilon_{LAD} = \frac{LAD_{mapped} - LAD_{modelled}}{LAD_{mapped}} \quad (6)$$

Inversion against Individual Landslides

The matching criterion followed herein aims at matching the modeled landslide location, area, and volume with those of the corresponding mapped landslide using an error minimization scheme for the centroid distance (ε_{CD}), area (ε_{Area}), and volume (ε_{Volume}) (Gong et al., 2023). An error of zero implies perfect match between the mapped and modeled landslide characteristic. Two inversions are run to explore the importance of landslide volume in inversion: one with volume data (ε_{Total_1}) and the other without volume data (ε_{Total_2}). The two total errors are calculated as:

$$\varepsilon_{Total_1}=\sqrt{\varepsilon_{CD}^2+\varepsilon_{Area}^2+\varepsilon_{Volume}^2} \quad (7)$$

$$\varepsilon_{Total_2}=\sqrt{\varepsilon_{CD}^2+\varepsilon_{Area}^2} \quad (8)$$

RESULTS

Inversion against Landslide Area Density

In the first set of inversions, the average landslide area density was matched. Figure 3 shows an example of the best-matching modeled landslides and the corresponding mapped landslides in Area 1. The modeled landslides shown correspond to a negligible relative error of 0.0027 between the modeled and mapped landslide area density. However, modeled landslides do not match the individual mapped landslides in location, number, and size. Three-hundred and thirty combinations of c', ϕ', R_u, and z resulted in very small relative errors in the range of 0-0.05 implying a near-perfect match between the modeled and mapped landslide area density. The corresponding effective normal stresses are plotted against the back-calculated shear strengths. The scatter in the data is significant, indicating a poorly defined regional strength envelope (Figure 4).

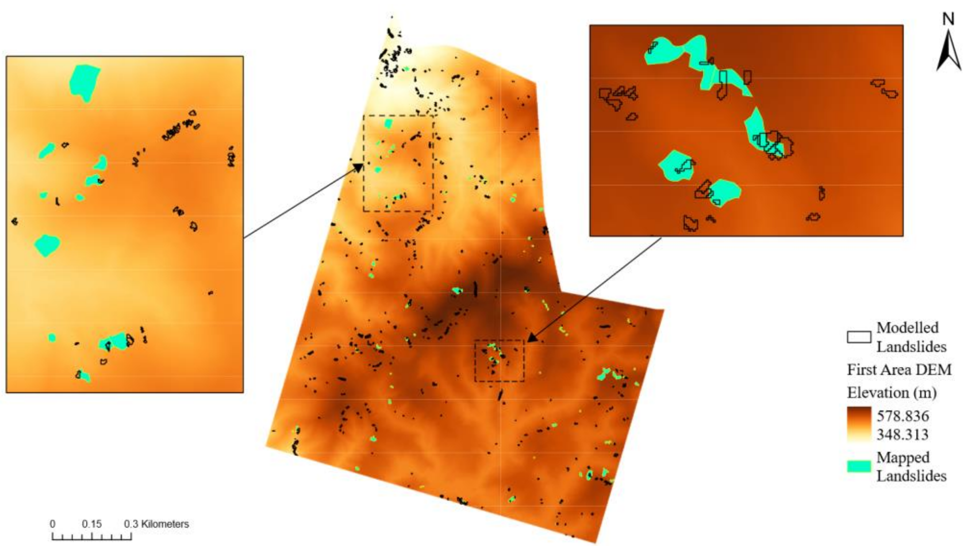

Figure 3. Inversion against landslide area density in Utuado region (Area 1)

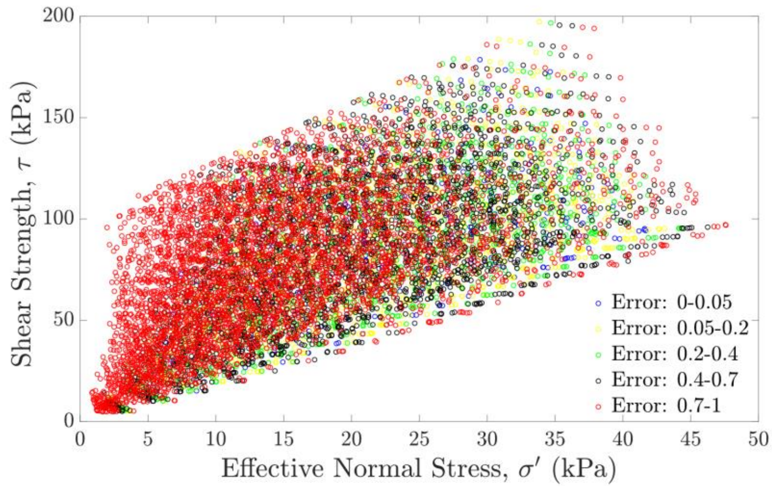

Figure 4: Shear strength versus normal stress (Inversion against landslide area density)

Inversion against Individual Landslides

Inversions were then conducted with the goal to invert individual mapped landslides in both Areas 1 and 2. Figure 5 shows the best-matching modeled landslides and the corresponding mapped landslides for Area 1. Results of inversion for Area 2 resemble those of Area 1and thus are not presented herein. The modeled landslides are represented using five color grades to reflect the degree of matching with the mapped landslides (i.e., the total error).

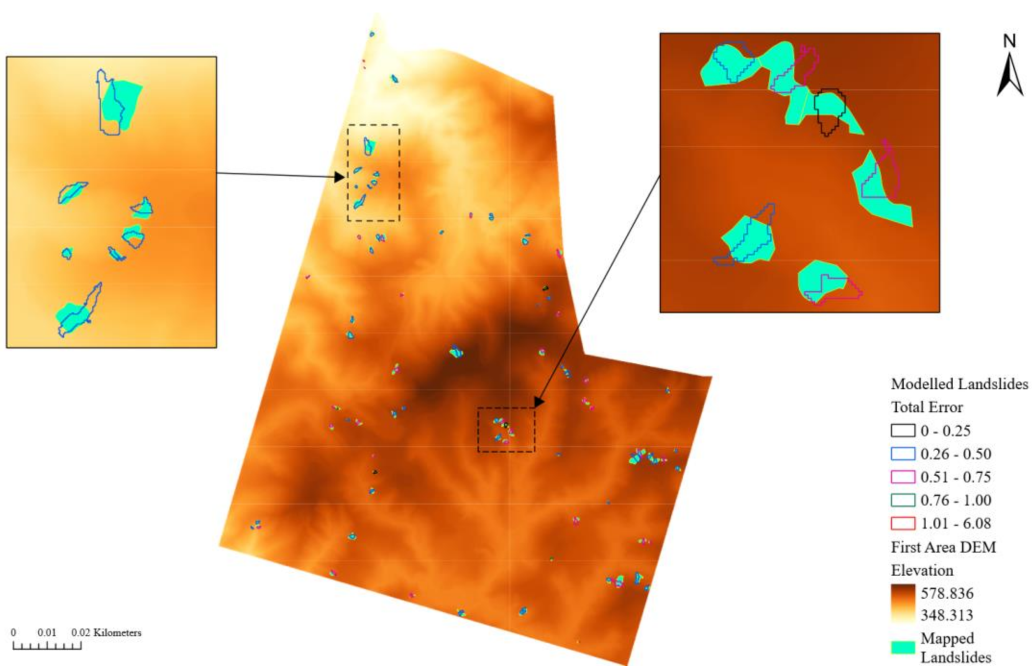

Figure 5. Inversion against individual landslides in Utuado region (First Study Area)

Figure 6 shows the frequency histograms of the total error, area error, volume error, and centroid distance error. Seventy-seven landslides have a total error of 0-0.25. On the other hand, only 13 landslides (~1.6% of the total landslides) have a total error >1. This demonstrates that the proposed inversion methodology is effective in inverting against rainfall-induced landslides. The 13 landslides with the highest total error (ε_{Total_1}>1) have relatively high centroid distance errors (0.97< ε_{CD} <1.96). Hence, the model in this case predicted landslides far away from the location of the mapped landslides. Out of the 788 landslides, 629 landslides (~80%) have underestimated areas (i.e., ε_{Area} < 0). Given that some mapped landslides could represent several smaller failing masses because of progressive failure, underestimating areas may be appropriate and may even possibly better represent the actual landslide failure mechanism. The results show good match in terms of the location with ~99% of the landslides having ε_{CD}< 1. The volume errors are more evenly distributed between over- and under-estimation with ~48% of the landslides having ε_{Volume}< 0. The over-estimated modeled volumes are because of the high modeled triggering depths compared to shallower mapped landslides.

Figures 7a and 7b show the distribution of the total errors against the mapped landslide areas and average calculated depths respectively. The average calculated depth is defined as the ratio of the volume calculated per Eq. (1) to the mapped landslide area. The highest total errors are recorded for smaller landslide areas. Hence, small landslides could be poorly matched by the model. This is not a resolution issue given that the DEM has a high resolution of 1m. Instead, this could be due to the model formulation which might not capture properly such failure mechansims. The highest total errors are also recorded for landslides that are shallower than 1m. Given that the DEM resolution is 1m, the model is unable to capture landslides shallower than this resolution.

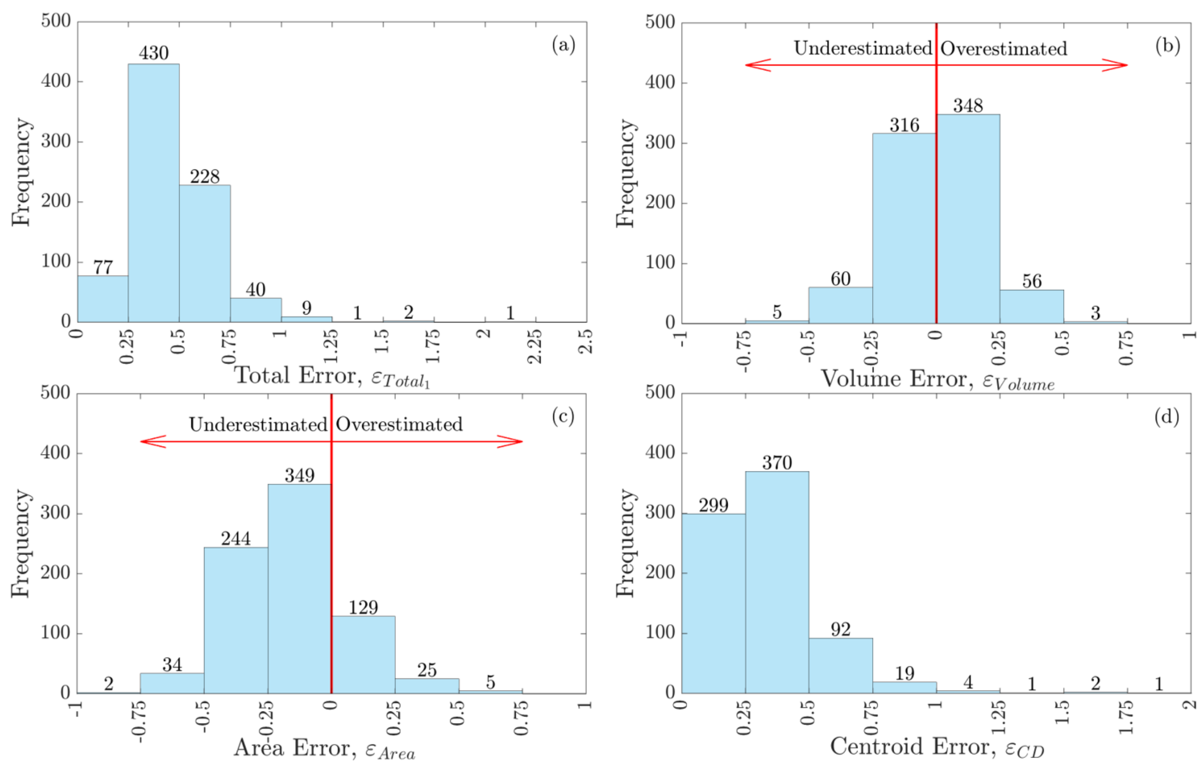

Figure 6. Distribution of (a) total error, (b) volume error, (c) area error, and (d) centroid distance error

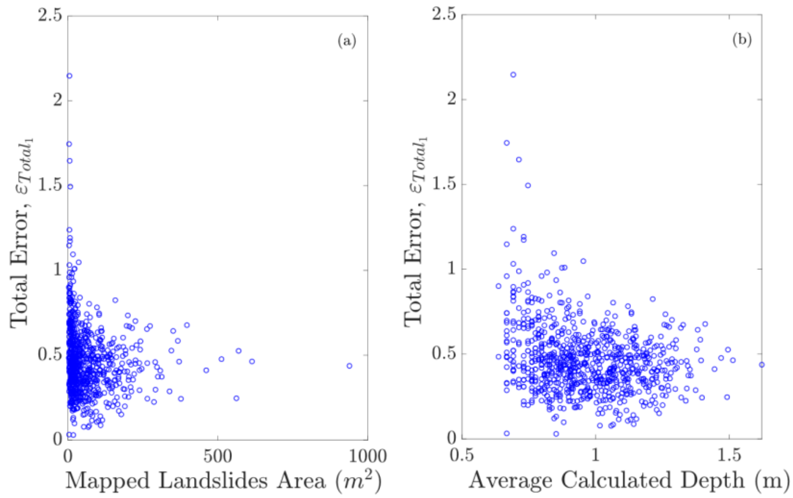

Figure 7. Total error against (a) mapped landslide areas and (b) average calculated depth

Normalized Shear Strengths

Larger landslides are likely to have higher strengths since the material is at higher confining stresses, and weathering should be lower at increasing depths. Thus, the back-calculated shear strength is normalized by the effective normal stress. Figure 8a shows the normalized shear strength against the mapped landslide areas. Higher normalized shear strengths ($\frac{\tau}{\sigma'} > 3$) are observed for smaller landslides with mapped areas less than 100 m^2. Larger landslides have a normalized shear strength that approaches a value of 1.3 (+/- 0.5). Higher normalized shear strengths are also observed at steeper slopes (Figure 8a). Figure 8b also shows an increasing exponential correlation between the topographic slope of the triggering grid cell and the normalized shear strength. This trend is expected not only mathematically, but also physically. High thickness of weathered material forming the soil mantle cannot stand at steeper slopes, and thus more intact material is observed that has higher strengths. At flatter slopes, the weathered material could be thicker with lower overall strength.

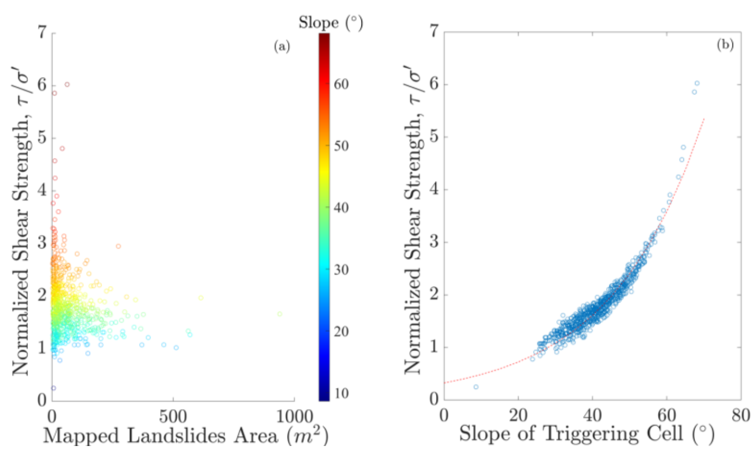

Figure 8. Normalized shear strengths against (a) mapped landslides area, and (b) slope of t triggering grid cell

Back-calculated Shear Strength Parameters

For each inverted landslide, the average effective normal stress and shear strength are calculated. Figure 9 shows the data pairs of normal stress and shear strength of inverted landslides with each landslide representing a data point. Landslides with a total error greater than 1 are omitted in this back-analysis. Because several combinations of c', ϕ', R_u, and z could result in the same minimum total error per each landslide, we show a measure of uncertainty in the shear strength for each data point. Uncertainty in the normal stress also exists but is not shown in the Figure. Figures 9a, 9b and 9c show the results for Area 1 without considering volume data in inversion, Area 1 with volume data, and Area 2 with volume data respectively.

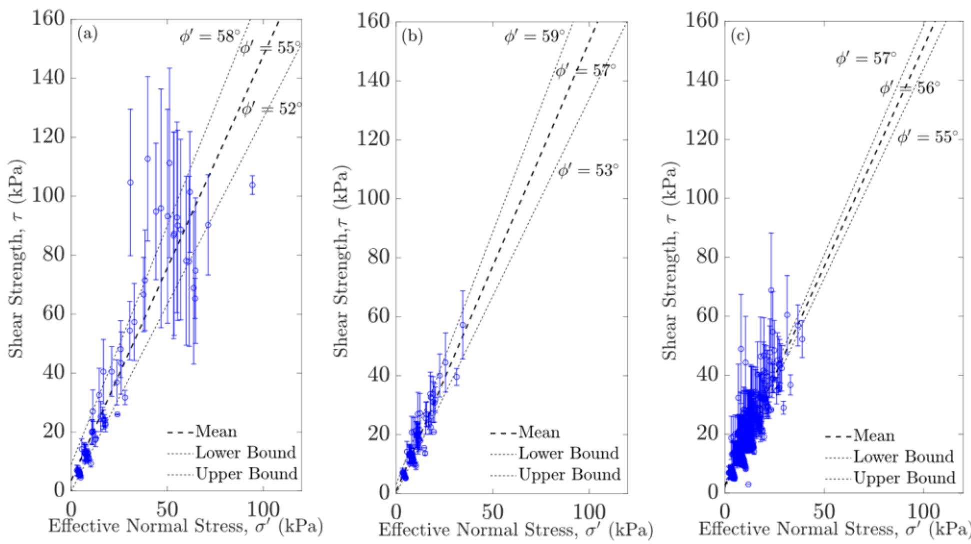

Figure 9. Fitting plot of shear strength against normal stress: (a) Area 1 without volume data, (b) Area 1 with volume data, and (c) Area 2 with volume data

A Mohr-Coulomb linear relationship is illustrated by the best-fit line for the data points (landslides). This linear regression gives an average cohesion of 4 kPa and average friction angle of 55° for the inversion without landslide volumes for Area 1, but also significant scatter in the data is observed. The cohesion varies between 0 and 9 kPa, and the friction angle varies between 52° and 58°. On the other hand, the back-calculated strength estimates derived from the inversion with landslides volumes are slightly different with an average cohesion of 1 kPa and an average friction angle of 57°. For inversion with volume data, the estimated friction angle varies between 53° and 59° and the cohesion varies between 0 and 3 kPa. As illustrated in Figure 9, inverting against landslide volumes reduces the uncertainty in the derived strengths. In addition, most data points in Figure 9b are concentrated at lower normal stresses compared to those in Figure 9a. This means that the modeled landslides are generally shallower when including volume data in the inversion analysis. This better matches the mapped landslides in this inventory which had an average failure depth of 1-2 m. Hence, inverting against volume data in addition to the mapped areas and centroids results in better matching of the mapped landslides. Figure 9c also shows the back-calculated shear strength estimates for the second area with volume data. The back-calculated cohesion varies between 2 kPa and 3 kPa while the friction angle varies between 55° and 57°. Although both study areas are in the same geologic unit, their strength parameters vary slightly. This variation could be reasonable because strengths are affected by various factors including topography, geomorphology, and hydrology even within the same geologic unit. This variation might also be a model limitation given that back-analysis is only conducted on failed slopes.

CONCLUSIONS

Inversion against individual landslides and against landslide area density have been performed based on a pseudo-3D methodology applied on 788 landslides caused by Hurricane Maria in the Utuado region in central Puerto Rico. The inversion results include polygons of best-matching modeled landslides to the mapped landslides. Inversion against landslide area density does a poor job in matching the location and size of the mapped landslides. This might indicate that either a regional average strength estimate is not appropriate using this inversion procedure or, more likely, that the model may need to be constrained more. On the other hand, inversion against individual landslides results in good match with mapped landslides. Inversion against individual landslides results in a reduced scatter of spatially distributed shear strength datapoints. Estimates of an average strength of each landslide and its variation are used to back-calculate cohesions and friction angles for the two study areas. The results show the importance of constraining the procedure with volume data to reduce the uncertainty in the estimated shear strengths and to model shallower landslides that match the actual failures. Matching small and shallow landslides was challenging although the DEM resolution was high. Higher normalized shear strengths were encountered at steeper slopes and for smaller landslides. Underestimation of the landslides' areas was high (~80%) possibly due to the effect of progressive failure where landslides fail in smaller parts rather than a single mass.

ACKNOWLEDGEMENTS

This study is partially funded by NASA through the Disasters program and Grants No. 80NSSC20K1032 and No. 80NSSC19K0948.

REFERENCES

Bishop, A. W., and Morgenstern, N. (1960). Stability coefficients for earth slopes. *Geotechnique*, 10(4), 129-153.

Duncan, J. M., Wright, S. G., and Brandon, T. L. (2014). *Soil strength and slope stability*. John Wiley & Sons.

Gallen, S. F., Clark, M. K., and Godt, J. W. (2015). Coseismic landslides reveal near-surface rock strength in a high-relief, tectonically active setting. *Geology*, 43(1), 11-14.

Godt, J. W., Baum, R. L., Savage, W. Z., Salciarini, D., Schulz, W. H., and Harp, E. L. (2008). Transient deterministic shallow landslide modeling: requirements for susceptibility and hazard assessments in a GIS framework. *Engineering Geology*, 102(3-4), 214-226.

Gong, W., Zekkos, D., and Clark, M. (2023). A pseudo-3D methodology for regional-scale back-analysis of earthquake-induced landslides. *Engineering Geology*, 107277.

Hughes, K. S., Bayouth García, D., Martínez Milian, G. O., Schulz, W. H., and Baum, R. L. (2019). Map of slope-failure locations in Puerto Rico after Hurricane María. US Geological Survey data release.

Hughes, K. S., and Schulz, W. (2020). Map depicting susceptibility to landslides triggered by intense rainfall, Puerto Rico (No. 2020-1022). US Geological Survey.
Schilirò, L., Esposito, C., and Scarascia Mugnozza, G. (2015). Evaluation of shallow landslide-triggering scenarios through a physically based approach: an example of application in the southern Messina area (northeastern Sicily, Italy). *Natural Hazards and Earth System Science*, 15(9), 2091-2109.
Segoni, S., Piciullo, L., and Gariano, S. L. (2018). A review of the recent literature on rainfall thresholds for landslide occurrence. *Landslides*, 15(8), 1483-1501.
USGS. (2017). 2015-2016 USGS Puerto Rico lidar: U.S. Geological Survey, accessed May 16, 2020, at ftp://rockyftp.cr.usgs.gov/vdelivery/Datasets/Staged/Elevation/OPR/PR_PuertoRico_2015/. (Access date: 07/01/2023).
USGS. (2020). Map data from landslides triggered by Hurricane Maria in four study areas in the Utuado Municipality, Puerto Rico, accessed May 16, 2020, at https://www.sciencebase.gov/catalog/item/5fb2b87ad34eb413d5e088e2. (Access date: 07/01/2023).


Geo-Congress 2024

GSP 349

Geotechnics of Natural Hazards

Selected Papers from Geo-Congress 2024
Vancouver, British Columbia, Canada | February 25–28, 2024

Edited by
T. Matthew Evans, Ph.D.
Nina Stark, Ph.D.
Susan Chang, Ph.D., P.E.

ASCE

GEO-INSTITUTE

GEOTECHNICAL SPECIAL PUBLICATION NO. 349

GEO-CONGRESS 2024

GEOTECHNICS OF NATURAL HAZARDS

SELECTED PAPERS FROM SESSIONS OF GEO-CONGRESS 2024

February 25–28, 2024
Vancouver, British Columbia, Canada

SPONSORED BY

The Geo-Institute
of the American Society of Civil Engineers

EDITED BY
T. Matthew Evans, Ph.D.
Nina Stark, Ph.D.
Susan Chang, Ph.D., P.E.

Published by the American Society of Civil Engineers